energies

MDPI

Article

Devolatilization of Residual Biomasses for Chemical Looping Gasification in Fluidized Beds Made Up of Oxygen-Carriers

Andrea Di Giuliano *, Stefania Lucantonio and Katia Gallucci

Department of Industrial and Information Engineering and Economics (DIIIE), University of L'Aquila, Piazzale E. Pontieri 1, Loc. Monteluco di Roio, 67100 L'Aquila, Italy; stefania.lucantonio@student.univaq.it (S.L.); katia.gallucci@univaq.it (K.G.)

* Correspondence: andrea.digiuliano@univaq.it; Tel.: +39-0862-434213

Abstract: The chemical looping gasification of residual biomasses—operated in fluidized beds composed of oxygen-carriers—may allow the production of biofuels from syngas. This biomass-to-fuel chain can contribute to mitigate climate change, avoiding the accumulation of greenhouse gases in our atmosphere. The ongoing European research project Horizon2020 CLARA (G.A. 817841) investigates wheat-straw-pellets (WSP) and raw-pine-forest-residue (RPR) pellets as feedstocks for chemical looping gasification. This work presents experimental results from devolatilizations of WSP and RPR, in bubbling beds made of three different oxygen-carriers or sand (inert reference), at 700, 800, 900 °C. Devolatilization is a key step of gasification, influencing syngas quality and quantity. Tests were performed at laboratory-scale, by a quartz reactor (fluidizing agent: N_2). For each pellet, collected data allowed the quantification of released gases (H_2, CO, CO_2, CH_4, hydrocarbons) and mass balances, to obtain gas yield (η^{av}), carbon conversion ($\chi^{av}{}_C$), H_2/CO ratio (λ^{av}) and syngas composition. A simplified single-first order-reaction model was adopted to kinetically analyze experimental data. WSP performed as RPR; this is a good indication, considering that RPR is similar to commercial pellets. Temperature is the dominating parameter: at 900 °C, the highest quality and quantity of syngas was obtained (WSP: η^{av} = 0.035–0.042 $mol_{gas}\ g_{biomass}{}^{-1}$, $\chi^{av}{}_C$ = 73–83%, λ^{av} = 0.8–1.0); RPR: η^{av} = 0.036–0.041 $mol_{gas}\ g_{biomass}{}^{-1}$, $\chi^{av}{}_C$ = 67–71%, λ^{av} = 0.9–1.0), and oxygen-carries generally performed better than sand. The kinetic analysis suggested that the oxygen-carrier ilmenite ensured the fastest conversion of C and H atoms into gases, at tested conditions.

Keywords: biomass; gasification; devolatilization; fluidized bed; oxygen carrier; biogenic residues; pellets

check for updates

Citation: Di Giuliano, A.; Lucantonio, S.; Gallucci, K. Devolatilization of Residual Biomasses for Chemical Looping Gasification in Fluidized Beds Made Up of Oxygen-Carriers. *Energies* **2021**, *14*, 311. https://doi.org/10.3390/en14020311

Received: 17 December 2020
Accepted: 6 January 2021
Published: 8 January 2021

Publisher's Note: MDPI stays neutral with regard to jurisdictional claims in published maps and institutional affiliations.

Copyright: © 2021 by the authors. Licensee MDPI, Basel, Switzerland. This article is an open access article distributed under the terms and conditions of the Creative Commons Attribution (CC BY) license (https://creativecommons.org/licenses/by/4.0/).

1. Introduction

The use of biomasses as a renewable feedstock has been investigated with great interest for producing energy and biofuels [1–4]. Several governmental programs have sustained this interest [1]: the European Union (EU) imposed to reach a 10% share of biofuels in the transport sector by 2020 [5]; in the USA, biofuels are expected to reach a production of 36 billion gallons by 2022 [6]. In the near future, so-oriented policies may represent a viable way to combine economic growth with the urgent need to oppose climate change, which was recently highlighted by the Paris agreement and the subsequent Conferences of the Parties to the United Nations Framework Conventions on Climate Change [1,7–10].

The chemical looping gasification for sustainable production of biofuels (CLARA) research project, funded by the EU Horizon 2020 framework program, G.A. 817841 [11] aims to contribute in this sense. This project deals with chemical looping gasification (CLG) of biogenic residues, with the obtained syngas used in the Fischer-Tropsch synthesis to produce liquid fuels, as also obtained by the hydrocracking of waxes resulting from Fischer-Tropsch. The main goal of CLARA is the realization of a full biomass-to-fuel chain up to 1 MWth scale, in an industrially relevant environment (targets: cold gas efficiency of 82%, carbon conversion of 98%, tar in outlet syngas lower than 1 mg Sm^{-3}) [11,12].

To our best knowledge, CLG has been operated only at laboratory scales up to 25 kW_{th} [13]. It couples the technologies of gasification [14] and chemical looping [15–19] thanks to solid particles of an oxygen-carrier (OC), which brings in the process the required oxygen to sustain endothermal gasification, avoiding air dilution. The CLG technology can consist of two coupled fluidized bed reactors, with OC particles which circulate from one to the other [11,20]: (i) in the fuel reactor, the OC bed is fluidized by steam and/or CO_2, while the biomass is gasified and the OC provides oxygen; (ii) the reduced OC leaves the fuel reactor with produced syngas, is separated by a cyclone and fed to the air reactor, where its re-oxidation occurs by combustion. The OC typically contains metal oxides [11]: in the CLARA project, Fe- [21–24] and Mn-based [16] materials were preferred over Ni- or Co-based ones, since the former are more environmental friendly [12].

With regard to the sustainability of CLG, the origin of biomasses is a key factor, since it can affect the degradation of agricultural lands, the forests reduction, the intensification of energy crops cultivation, and their competition against food and feed [12,25]. For these reasons, only residual biomasses (i.e., biogenic residues) have been considered in the CLARA project, as they do not alter the food chain; however, quality and competitiveness of residual biomasses must be improved to properly introduce them into the market [12,26–28]. Cereal straw is attractive, as it its largely available: its estimated quantity is close to the sum of forest and non-forest woody residues [29].

This work descends from researches of the CLARA project, regarding the devolatilization of residual biomasses (residues of wheat straw and raw pine forest), carried out at laboratory-scale in fluidized beds made up of different OCs.

Devolatilization is a key step of the gasification process, and strongly influences both quantity and quality of obtained syngas [30]. At the temperatures of gasification (typically up to 900 °C), vapors and tars—developed by primary devolatilization reactions, undergo secondary reactions, which contribute to both gaseous products (cracking and reforming) and solid products (polymerization) [30,31]. According to the reactor configuration, the steps of gasification process (pre-heating and drying, devolatilization or pyrolysis, gasification, combustion) can occur in well separated zones at different temperatures or without a clear spatial distinction [32]. As far as fluidized bed gasifiers are concerned, there are not separated reaction zones in the bed and the process is isothermal [32]; by contrast, an abrupt transition occurs to the fed particles of solid fuel [30,33]. This transition involves [30,33]: (i) a rapid heating from room feeding temperature to that of the gasifier bed; (ii) simultaneous drying, devolatilization and secondary reactions; (iii) fluid-dynamic interactions among fluidizing/gasification agents (e.g., steam, air), bed particles, fuel particles, reaction products; (iv) morphological changes of solid fuel particles, due to phenomena at points (i), (ii) and (iii).

In the light of these peculiarities of solid/gas mixing, assessments and predictions about biomass behavior in industrial fluidized beds should be based on experimental data in the same kind of reactors; extrapolations from data obtained under different experimental conditions (e.g., laboratory thermogravimetric analyses) could turn out to be unreliable [30,34–36].

This work aims to provide useful experimental data about the devolatilization of residual biomasses in bubbling beds, made up of three different OC (selected for CLG within the CLARA project) or sand (as a reference material). Pellets of raw wheat straw and raw pine forest residues were investigated, and their devolatilization performances were evaluated in terms of average gas yield per unit of biomass mass, carbon conversion, gas composition, H_2/CO ratio: effects from temperature (in the range 700–900 °C), biomass origin and bed material were evaluated and discussed, also thanks to a simplified kinetic analysis.

Collected results have an important novelty value for both experimental and modelling studies, since they deal with: (i) residual biomasses with a great availability potential, nowadays unexploited; (ii) devolatilization, a single step of the more complex gasification process, tricky to be experimentally isolated especially at higher scales; (iii) formulation of kinetic expressions of devolatilization/pyrolysis, a crucial point, often lacking, for a

full-predictive modeling approach; (iv) chemical looping gasification by means of OCs, a thermochemical process which has not been developed yet at industrial scale.

2. Materials and Methods

2.1. Biomasses

In the framework of the CLARA project, two biogenic residues were chosen, since they were largely available and potentially usable in Europe and worldwide: residues of wheat straw and raw pine forest, both collected in Navarra (North of Spain). Pellets of these biomasses were investigated in this work, produced by the National Renewable Energy Centre of Spain (CENER), a partner of the CLARA project, according to methods and by devices described elsewhere [12,37]. The pellets diameter was 6 mm. From here on, they are named WSP (wheat straw pellets) and RPR (raw pine residue pellets).

Within the research project CLARA, these pellets were characterized (proximate and ultimate analyses, available elsewhere [38]), obtaining contents of moisture (weight percentage on as received basis, $\%moisture_{ar}$), ashes (weight percentage on dry basis, $\%ash_{db}$), carbon and hydrogen (weight percentage on dry ash-free basis, $\%C_{daf}$ and $\%H_{daf}$). These quantities were used for the calculations of this work.

2.2. Bed Materials

Chalmers University of Technology (Göteborg, Sweden), another partner of the CLARA project, had kindly provided the three OCs used as bed materials for the devolatilization tests: ilmenite (iron–titanium-based mineral) [39], calcined Sibelco (manganese–iron-based mineral), and LD-slag (iron–manganese–calcium-based by-product) [40]. For the sake of brevity, from here on, they were respectively named ILM, SIB, LD.

The same tests were also carried out with a bed made up of sand, used as a reference, for comparisons with the three OCs.

Table 1 summarizes the properties of interest for the fluid-dynamic evaluation of all bed materials. According to these values, each bed material was associated to the corresponding generalized Geldart group [41] at the experimental conditions of devolatilization tests. With N_2 at 700 °C, 800 °C and 900 °C (see Section 2.3), they all belonged to Group B (bubbling), i.e., they could not provide homogeneous fluidization [41]. In general, minimum fluidization and bubbling fluidization velocities coincide for Group B [41]. For the sake of clarity, from here on, the term "minimum fluidization velocity (u_{mf})" was used to define the lowest superficial velocity at which bubbling fluidization begins for each of the three OCs and for sand.

Table 1. Properties of fluid-dynamic interest and related minimum fluidization velocities of all bed materials, as functions of temperature (adapted from [12] for the OCs).

	Sand	**ILM**	**SIB**	**LD**
d_p [1] (μm)	231	255	208	235
ρ_p [2] (kg m^{-3})	2587	3830	3770	2676
T (°C)	u_{mf} [3] (cm s^{-1})	u_{mf} [3] (cm s^{-1})	u_{mf} [3] (cm s^{-1})	u_{mf} [3] (cm s^{-1})
700	2.4	4.4	2.9	2.6
800	2.3	4.1	2.7	2.4
900	2.1	3.8	2.5	2.3

[1] $d_{[3,2]}$ determined by Malvern Mastersizer 2000. [2] Determined by comparison with known granular material. [3] Calculated by the semiempirical correlation presented in [12], with correlation constants C1 = 27.2 and C2 = 0.0408 [42,43].

2.3. Devolatilization Experiments

Devolatilization tests were performed at 700 °C, 800 °C and 900 °C, to observe the instantaneous pyrolysis behavior of WSP and RPR in bubbling fluidized beds made up of one OC or sand. The laboratory-scale experimental apparatus (Figure 1) included one

reactor made of quartz (5 cm internal diameter), placed in a cylindrical electric furnace, and fed upward by N_2 (carrier gas and fluidizing agent at 1.5 u_{mf}).

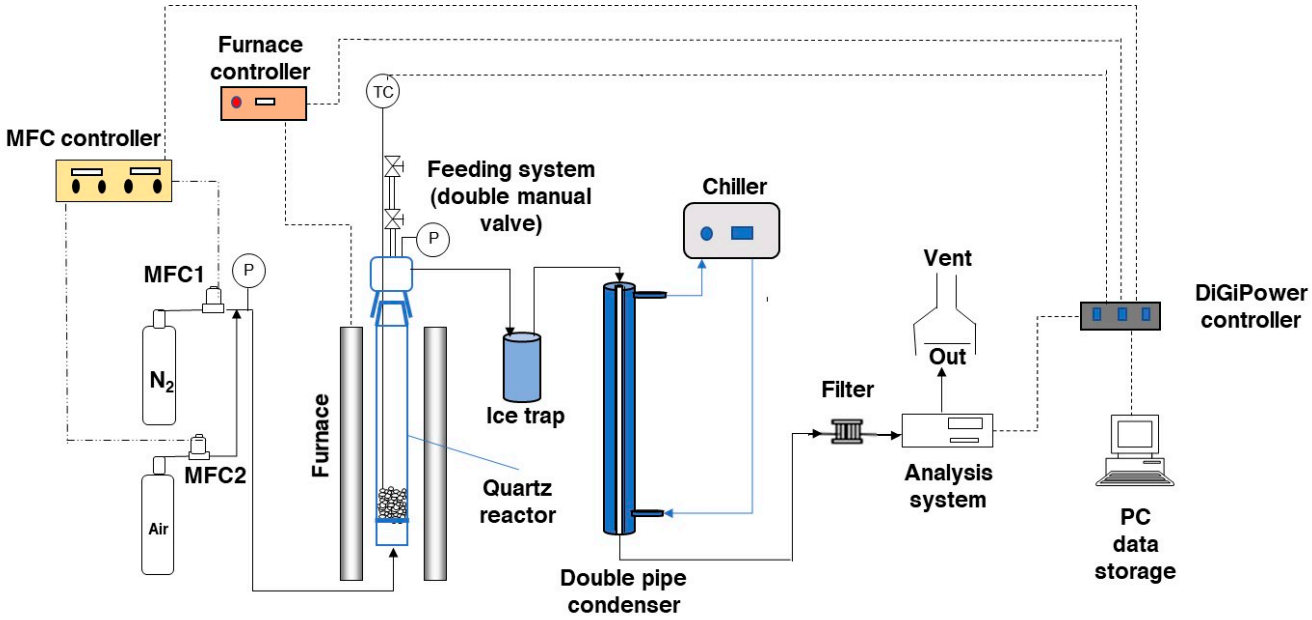

Figure 1. Schematic view of the laboratory-scale experimental apparatus for pyrolysis tests.

A sintered porous quartz plate sustained the fluidized bed and served as a gas distributor. The bottom part of the reactor, underneath this quartz plate, was filled by a packed bed made of SiC particles; this bulk of SiC was placed inside the furnace, so to work as a preheater for the fluidizing N_2 flow. The masses of loaded OCs or sand were selected in order to obtain 7.5 cm high beds (1.5 times the bed diameter).

The temperature of the bed was controlled by a K-type thermocouple, protected by a quartz socket and submerged in the bed. Devolatilization products and N_2 left the reactor from its top, passed through an ice trap and a double-pipe glass condenser (cooled by diethylene glycol at about 0 °C), to be then analyzed by an ABB online system (ABB S.p.A., Sesto San Giovanni (MI), Italy) and by a micro-gas chromatograph (μGC) (Agilent 490, Agilent Technologies Italia S.p.A., Cernusco sul Naviglio (MI), Italy).

The ABB system included an ADVANCE OPTIMA URAS 14 module for CO, CO_2, CH_4 (non-dispersive infrared detector, NDIR), an ADVANCE OPTIMA CALDOS 17 module for H_2 (thermal conductibility detector, TCD), and an ADVANCE OPTIMA MULTI-FID14 (flame ionization detector, FID) for hydrocarbons. Concentrations of CO, CO_2, CH_4 and H_2 were measured as vol%, while the overall hydrocarbons content was expressed as ppm_v of equivalent C_3H_8. The Agilent 490 μGC system was equipped in order to identify: ethane, ethylene/acetylene, propane, propene, propadiene, propyne, *n*-butane, isobutane, *n*-pentane, isopentane, neopentane, *n*-hexane, benzene and toluene. These species could contribute to the total hydrocarbons quantified by the FID. For each tested pellet, one μGC analysis was performed on the stream of dry product gases thanks to a single sampling injection per test.

Biomass pellets were fed individually by hand, thanks to a vertical double-valve system over the reactor top (Figure 1), at room temperature: (i) the upper valve was opened to load the pellet, while the lower one remained closed to isolate the reaction environment; (ii) the upper valve was closed to isolate the reaction environment, then the lower one was opened to make the pellet fall into the bed. This manual system allowed to make the pellet experience a temperature transition similar to that of industrial feeding, i.e., an abrupt switch from room temperature up to that of the bed. This was not possible by more usual equipment, such as thermogravimetric analyzers.

For each set "biomass kind/bed material/bed temperature", three repetitions of individual pellet devolatilization were performed. The devolatilization of one pellet was carried out until completion, before feeding the following; as a consequence, the process was in unsteady-state.

Outlet molar flow rates ($F_{i,out}$) were determined as functions of time (t) for produced H_2, CO, CO_2, CH_4 and equivalent C_3H_8, thanks to ABB measurements and assuming the N_2 inlet flow rate as the internal standard. Values of $F_{i,out}$, individual pellet masses (m_p) and biomass composition [38] allowed the calculation of integral-average values of: gas yield (η^{av}, Equation (1)), percentage composition on dry and dilution-free basis ($Y^{av}{}_i$, Equation (2)), carbon conversion ($\chi^{av}{}_C$, Equation (3), with n_j as the number of C atoms in j), outlet H_2/CO molar ratio (λ^{av}, Equation (4)). For each set "biomass kind/bed material/bed temperature", average values of the three repetition were calculated for η^{av}, $Y^{av}{}_i$, $\chi^{av}{}_C$, and λ^{av}, provided with related standard deviations:

$$\eta^{av} = \frac{\sum_i \int F_{i,out}\, dt}{m_p} \quad \text{with } i = H_2,\ CO,\ CO_2,\ CH_4 \text{ and equivalent } C_3H_8 \tag{1}$$

$$Y_i^{av} = \frac{\int F_{i,out}\, dt}{\sum_i \int F_{i,out}\, dt} 100 \quad \text{with } i = H_2,\ CO,\ CO_2,\ CH_4 \text{ and equivalent } C_3H_8 \tag{2}$$

$$\chi_C^{av} = \frac{\left(12\ \mathrm{g\ mol^{-1}}\right) \times \sum_j \left(n_j \int F_{j,out}\, dt\right)}{m_p \left(1 - \frac{\%moisture_{ar}}{100}\right)\left(1 - \frac{\%ash_{db}}{100}\right)\left(\frac{\%C_{daf}}{100}\right)} 100 \quad \text{with } j = CO,\ CO_2,\ CH_4 \text{ and equivalent } C_3H_8 \tag{3}$$

$$\lambda^{av} = \frac{\int F_{H_2,out}\, dt}{\int F_{CO,out}\, dt} \tag{4}$$

2.4. Kinetic Parameters for Devolatilization in Fluidized Beds

The proposed modelling approach (see Appendix A) was based on some simplifying hypotheses, so to provide a simple tool for evaluations in the context of this work, tailored to the kind of data obtained by the experimental procedure described in Section 2.3.

In general, the different reaction zones of biomass devolatilization—which correspond to the decomposition of biomass components—tend to merge with more severe heating conditions [44]; therefore, when fast heating rate or high temperature conditions occur (like in this work), the devolatilization mechanism consists of a one-stage decomposition, made up of three parallel reactions: three lumped products are involved (char, liquid and tars, gases) [44], according to the scheme proposed by Shafizadeh and Chin [45] for wood (Figure 2).

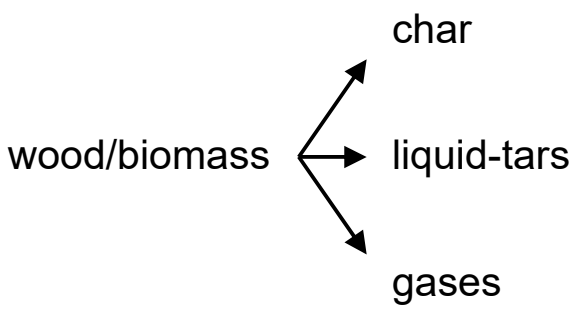

Figure 2. One-component mechanism of devolatilization by Shafizadeh and Chin [45], adapted from [44].

For this mechanism, the single first order reaction (SFOR) model is usually adopted [44,46,47] as generalized in Equation (5), where $w(t)$ is the mass fraction of biomass (i.e., all the biomass not transformed in char, liquid-tars, gases) as a function of time (t), and k is the specific reaction rate expressed by an Arrhenius-type function:

$$\frac{dw(t)}{dt} = -k\, w(t) \tag{5}$$

$$k = A \cdot \exp\left(-\frac{E_a}{R\,T}\right) \tag{6}$$

In this work, the SFOR model was adapted to the nature of available experimental devolatilization data. The adapted model (see Appendix A) allowed the determination—for each bed material—of specific reaction rates for the conversion of C and H atoms from biomass into gas products H_2, CO, CO_2, CH_4. These specific reaction rates were named k_C and k_H, respectively.

Thanks to experiments at three temperature levels (T), pre-exponential factors (A_C and A_H) and activation energies ($E_{a,C}$ and $E_{a,H}$) were calculated from values of k_C and k_H, for each couple "biomass kind/bed material". Readers should refer to Appendix A for further details.

3. Results

Figure 3 shows examples of gas produced by devolatilizations of individual pellets, evidencing the intrinsic unsteady-state of the monitored process: devolatilization products were released in the carrier gas and transported to the analyzers, determining the characteristic peak form of the calculated outlet molar flowrates ($F_{i,out}$). As previously verified in the same laboratory of this work [30], an experimental system as the one described in Section 2.3 generates a flow-mixing which is reasonably well modeled as a perfect mixer (reactor) together with plug flow (transport lines to the analyzers). As to $F_{i,out}$ curves of H_2, CO, CO_2, CH_4, the lag time related to transmission lines was eliminated by the data treating process; on the other hand, the peak of $F_{C3H8,out}$ presented a systematic delay in comparison to others. This depends on the position of the sampling point of MULTI-FID 14: it was placed at the very end of the experimental apparatus, just before the vent of the product gases, therefore after these gases had already passed through all other analyzers.

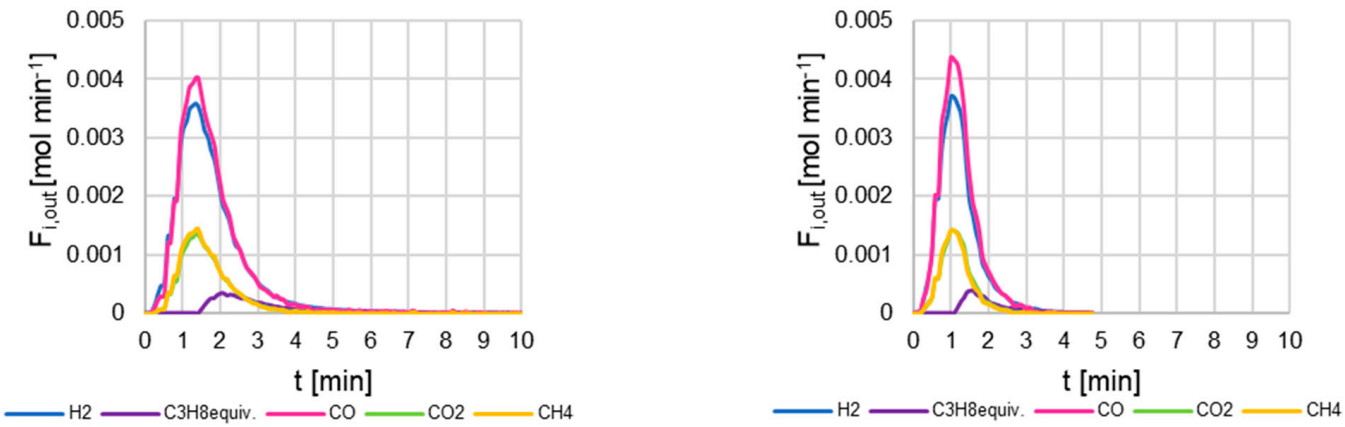

(**a**) (**b**)

Figure 3. *Cont.*

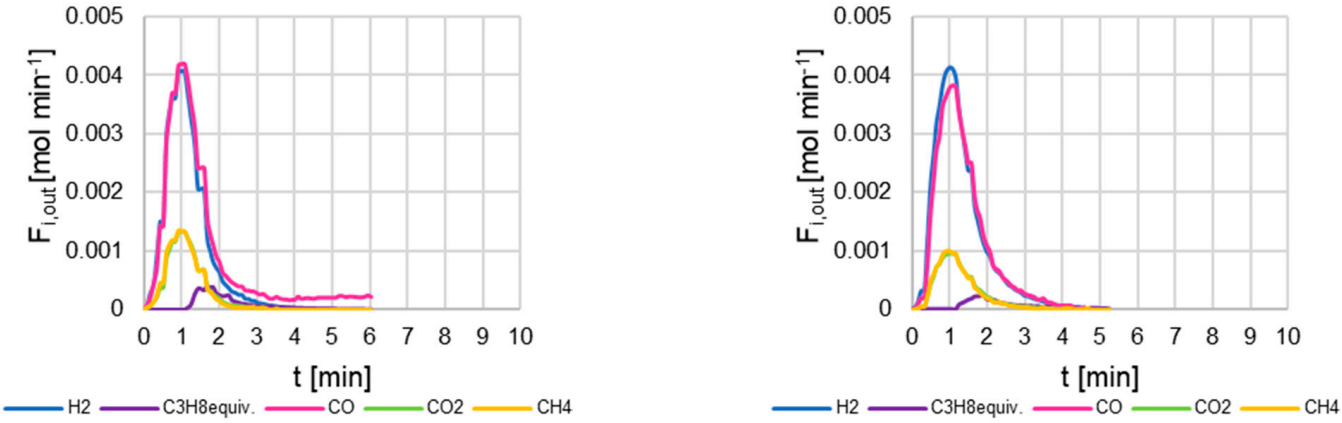

Figure 3. Example of H_2, CO, CO_2, CH_4 and equivalent C_3H_8 outlet molar flow rates ($F_{i,out}$) as functions of time (t), produced by devolatilizations of individual WSP pellets at 900 °C in beds made of sand (**a**), ILM (**b**), SIB (**c**) and LD (**d**).

The integration of those peaks with respect to time allowed the calculation of mass balances for each tested pellet, and then the quantification of results summarized in Figures 4 and 5, according to the procedure described in Section 2.3. Figure 4 compares all integral-average gas yields (η^{av}, Equation (1)), carbon conversions ($\chi^{av}{}_C$, Equation (3)) and outlet H_2/CO molar ratios (λ^{av}, Equation (4)). Figure 5 does the same for integral-average compositions ($Y^{av}{}_i$, Equation (2)) of produced H_2, CO, CO_2, CH_4 and equivalent C_3H_8. Numerical data represented in Figures 4 and 5 were reported in the Appendix **??** of this work. For each individual devolatilization, one online sampling of produced gas was carried out by the µGC AGILENT 490; for the sake of brevity, results are not detailed in this work, but just discussed in Section 4.

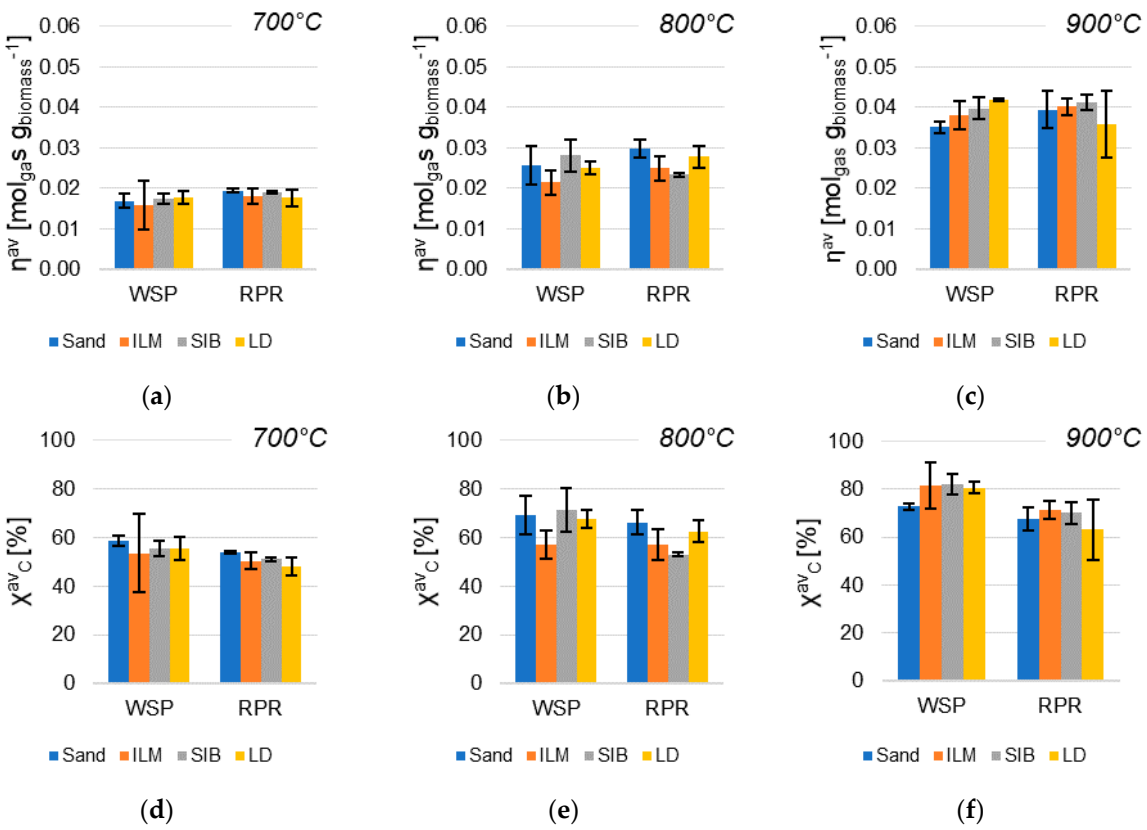

Figure 4. *Cont.*

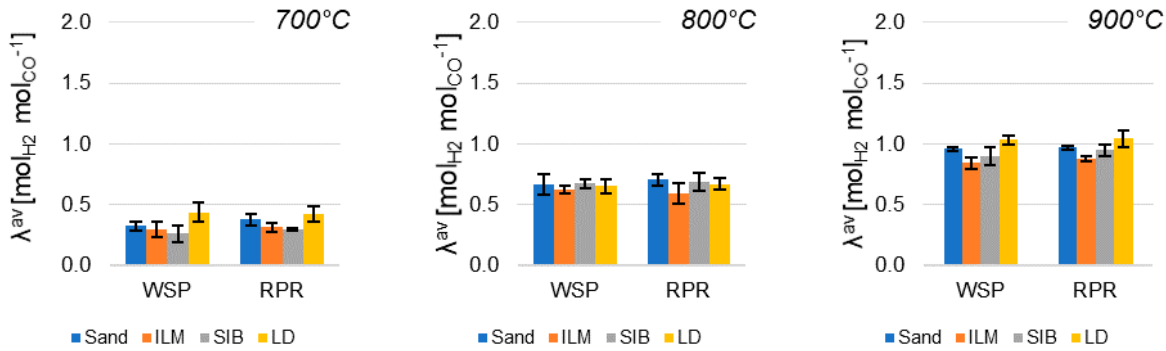

(**g**) (**h**) (**i**)

Figure 4. Experimental results of devolatilization tests as functions of temperature, kind of biomass, kind of bed material: integral-average gas yield (η^{av}, Equation (1)) at 700 °C (**a**), 800 °C (**b**), 900 °C (**c**); integral-average carbon conversion ($\chi^{av}{}_C$, Equation (3)) at 700 °C (**d**), 800 °C (**e**), 900 °C (**f**); integral-average H_2/CO molar ratio (λ^{av}, Equation (4)) at 700 °C (**g**), 800 °C (**h**), 900 °C (**i**).

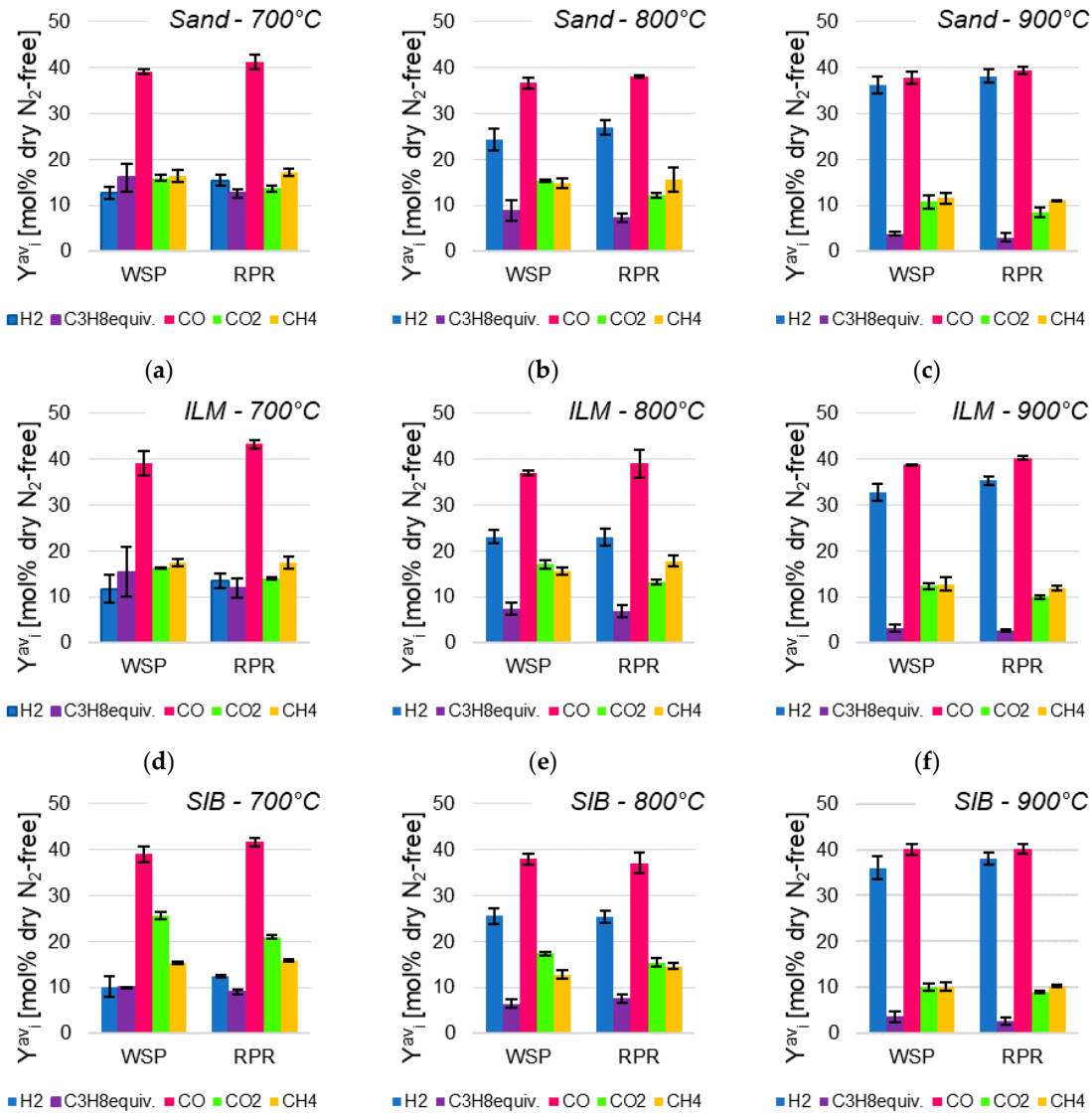

(**a**) (**b**) (**c**)

(**d**) (**e**) (**f**)

(**g**) (**h**) (**i**)

Figure 5. *Cont.*

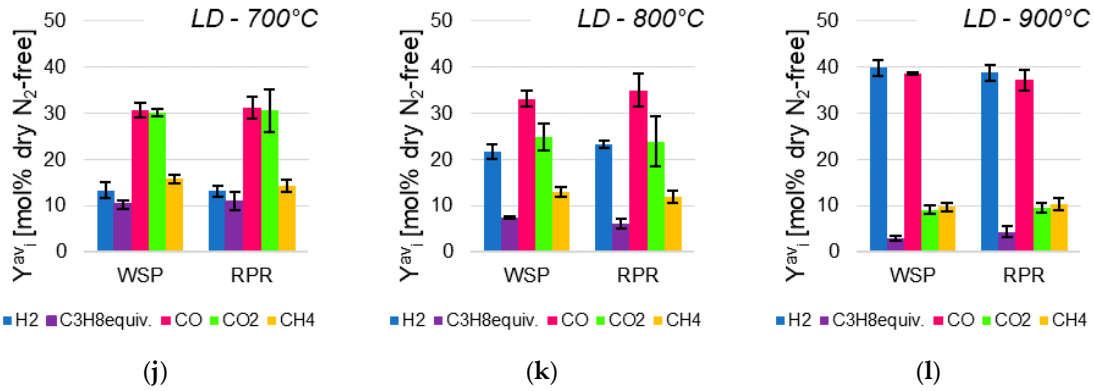

Figure 5. Experimental integral-average composition of gas from devolatilization tests as functions of temperature, kind of biomass, kind of bed material, expressed as mol% dry and dilution-free ($Y^{av}{}_i$, Equation (2)): sand at 700 °C (**a**), 800 °C (**b**), 900 °C (**c**); ILM at 700 °C (**d**), 800 °C (**e**), 900 °C (**f**); SIB at 700 °C (**g**), 800 °C (**h**), 900 °C (**i**); LD at 700 °C (**j**), 800 °C (**k**), 900 °C (**l**).

According to the procedure described in Appendix A, the values of H_2, CO, CO_2, CH_4 outlet molar flowrates ($F_{i,out}$) were also used to determine the specific reaction rates k_C and k_H, representative of the overall conversion of C and H atoms from biomass into gas products; kinetic constants related to the different temperature levels allowed the calculation of pre-exponential factors (A_C and A_H) and activation energies ($E_{a,C}$ and $E_{a,H}$). Values of k_C and k_H are in Appendix **??** of this work, while Table 2 summarizes the obtained values of A_C, A_H, $E_{a,C}$ and $E_{a,H}$.

Table 2. Pre-exponential factors and activation energies calculated from devolatilization data according to the procedure described in Appendix A.

	WSP				RPR			
	A_C	$E_{a,C}$	A_H	$E_{a,H}$	A_C	$E_{a,C}$	A_H	$E_{a,H}$
	(min^{-1})	(kJ mol^{-1})	(min^{-1})	(kJ mol^{-1})	(min^{-1})	(kJ mol^{-1})	(min^{-1})	(kJ mol^{-1})
Sand	4.1	19.1	65.6	45.2	3.3	18.1	54.4	43.2
ILM	11.1	24.6	102.2	46.4	6.9	21.9	100.5	46.6
SIB	6.1	20.1	390.8	58.9	3.1	15.7	197.2	53.3
LD	9.1	25.3	460.2	61.2	7.3	24.2	258.3	56.6

4. Discussion

4.1. Experimental Data

As a first point for this discussion, it is worth to stress that the reactor feed was anoxic and dry (pure N_2), so the main sources of oxygen are the bed, when OCs are used, and the biomass. As a consequence, the presence of oxidized carbon in gases (CO and CO_2, see Figure 5) is due to the solids involved in the process.

Some general effects due to temperature emerged from the results presented in Section 3. As can be seen in Figure 4, for all bed materials (sand, ILM, SIB, LD) and both biomasses (WSP and RPR) integral-average gas yields (η^{av}, Equation (1), Figure 4a–c), carbon conversions ($\chi^{av}{}_C$, Equation (3), Figure 4d–f) and H_2/CO ratios (λ^{av}, Equation (4), Figure 4g–i) increased as the temperature was increased from 700 °C to 900 °C. As to integral-average gas composition ($Y^{av}{}_i$, Equation (2), Figure 5), whatever the bed material or the converted biomass, concentrations of CO_2, CH_4 and equivalent C_3H_8 decreased as the temperature was increased, while that of H_2 concomitantly became higher; this could be ascribed to the enhancement of hydrocarbons decomposition (thermal cracking or reforming reactions), while the decrease of CO_2 could be ascribed to a the lower extent of exothermic reactions (combustion and water gas shift). CO did not show relevant trends of variation with temperature. The measurements of µGC generally agreed with trends of equivalent C_3H_8 (especially data related to sand). In addition, they suggested that the equivalent C_3H_8 contained hydrocarbons among those detectable by the µGC (see Section 2.3); for instance, at 700 °C with sand, peaks with retention times

compatible to all detectable hydrocarbons appeared at least once, except for *n*-hexane, toluene, propadiene and propene; at 800 °C with sand, only peaks compatible with ethylene/acetylene, ethane, *n*-butane and benzene were found, while at 900 °C no hydrocarbons were identified. With OCs, only benzene and C_4 hydrocarbons were occasionally identified. In any case, the μGC analyses must be considered only as an optional support to the identification of hydrocarbons quantified by the FID detector; the fact that the sampling was started manually, during an intrinsically unsteady process, imposes to use caution in the interpretation of μGC results.

Less clear-cut trends could be ascribed to the different kinds of biomass or OCs; still, some evidences could be commented.

WSP and RPR did not show performances of devolatilization with dramatic differences, as far as gas quantity (η^{av}, Figure 4a–c) and quality (λ^{av}, Figure 4g–i and $Y^{av}{}_i$, Figure 5) are concerned. More in detail, slightly higher carbon conversion ($\chi^{av}{}_C$, Figure 4d–f) generally occurred for WSP. These were good process indications for the CLG of residual biomasses, since RPR could be considered as close to the current commercial reference of wood pellets; the fact that WSP had devolatilization performances similar to RPR corroborated WSP eligibility for the CLG, even though other factors should be taken into account (e.g., agglomeration tendencies of ashes in fluidized beds [12,48]).

With regard to WSP, when comparing the performance of OCs to that of sand, the action of OCs was exalted by the increase of temperature in terms of integral-average gas yield (η^{av}, Figure 4a–c and Table A1) and carbon conversion ($\chi^{av}{}_C$, Figure 4d–f and Table A1): these quantities for sand and OCs were comparable at 700 °C (Figure 4a,d and Table A1) and 800 °C (Figure 4b,e and Table A1), while the OCs generally ensured higher values at 900 °C (Figure 4c,f and Table A1). With regard to RPR, once standard deviation were taken into account for gas yields (Figure 4a–c and Table A2) and carbon conversions (Figure 4d–f and Table A2), less important effects due to the bed material emerged. For both biomasses, Figure 4g,i suggest that LD slightly improved the H_2/CO ratio when compared to sand; this could be explained by the fact that LD can be involved in water-splitting reactions, thanks to wüstite-structures [49].

As far as integral-average gas compositions are concerned ($Y^{av}{}_i$, Equation (2)), some differences due to the OCs could be enucleated only at 700 °C (Figure 5a,d,g,j, Tables A1 and A2): SIB and LD increased the fraction of CO_2 in comparison to sand and ILM. Nevertheless, at 900 °C the distribution of gas components became very similar for all bed materials and biomasses (Figure 5c,f,i,l).

After this overall evaluation of the experimental data, 900 °C appeared as the most recommendable temperature to operate the thermal decomposition of both WSP and RPR, as it maximized gas yield (η^{av}, Equation (1)), carbon conversion ($\chi^{av}{}_C$, Equation (3)) and the H_2/CO molar ratio (λ^{av}, Equation (4)), whatever the used bed material (WSP: η^{av} = 0.035–0.042 $mol_{gas}\ g_{biomass}{}^{-1}$, $\chi^{av}{}_C$ = 73–83%, λ^{av} = 0.8–1.0); RPR: η^{av} = 0.036–0.041 $mol_{gas}\ g_{biomass}{}^{-1}$, $\chi^{av}{}_C$ = 67–71%, λ^{av} = 0.9–1.0). At 900 °C:

- C of WSP resulted as slightly more converted into gases than C of RPR, while all other performance parameters could be considered very close;
- in general, OCs incremented gas yield and carbon conversion in comparison to sand (the average values of the LD/RPR couple were lower than those of sand, but affected by a significative standard deviation);
- the values of the molar H_2/CO ratio (close to or equaling 1) were promising, since this work dealt with devolatilizations: with steam as a gasifying agent in a CLG process, one would expect to get higher H_2/CO ratios, closer to the target of 2, which is ideal for the Fischer-Tropsch synthesis hypothesized in the biomass-to-fuel chain of the CLARA project. In this specific regard, LD appeared as the most interesting OC, as it was the only one ensuring a molar H_2/CO ratio higher than that of sand, with both WSP and RPR.

4.2. Kinetic Analysis

As stated by Kersten et al. [50] in their Part I of a review about biomass devolatilization in a fluidized bed reactor, "*there is wide variation in data published for combined values of the preexponential factor and activation energy. Published rate and selectivity expressions may be valuable in describing trends, but they can hardly ever be used for reliable quantitative prediction of anything else than the corresponding original data*". In the light of this statement, only trends due to the kinetic parameters in Table 2 were analyzed, only for comparisons among the materials studied in this work.

Kinetic parameters in Table 2 must be intended as apparent, i.e., they lumped external heat transfer from bed to pellet, internal heat transfer inside the pellet, intrinsic devolatilization kinetics (in turn according to the one-component reaction scheme in Figure 2). As a matter of facts, in their Part II of the abovementioned review, Wand et al. [51] noted that "*for the biomass particle sizes applied in practical reactors, from 1 to 5 mm, the pyrolysis time is influenced by all three mechanisms: the pyrolysis kinetics, the heat transfer from the bulk of the reactor to the particle, and the intraparticle heat conduction*". Pellets of this work could be reasonably included in this case.

The specific reaction rates k_C and k_H, recalculated by Equation (6) and parameters in Table 2, helped to reabsorb part of the experimental variabilities obtained pellet by pellet (see Tables A3 and A4). Calculated k_C and k_H were interpreted as characteristic conversion frequencies of C and H, at a given temperature and at 1.5 u_{mf}. For both WSP and RPR, k_C and k_H of OCs were higher than those of sand, suggesting a general benefic effect of OCs towards the conversion of biomass pellets into gases, inside a bubbling bed. With regard to C, both WSP and RPR had the highest specific reaction rates with ILM, at 700, 800 and 900 °C (e.g., at 900 °C, WSP: k_C = 0.88 min^{-1} with ILM vs. k_C = 0.58 min^{-1} with sand; RPR: k_C = 0.72 min^{-1} with ILM vs. k_C = 0.52 min^{-1} with sand). The same occurred with H, except for the SIB/WSP couple at 900 °C, even though greater than that of ILM/WSP by only 0.05 min^{-1}.

For each couple "biomass/bed material", H activation energy ($E_{a,H}$, Table 2) was higher than C one ($E_{a,C}$, Table 2): this matched well with the fact that integral-average H_2 fraction in the product gas was always the most affected by temperature increase ($Y^{av}{}_{H2}$, Figure 5).

5. Conclusions

Once considered that RPR is close to current commercial biomass pellets, WSP resulted as a convincing alternative for thermochemical conversions, since the two biomasses always showed very similar devolatilization performances at the investigated conditions, in terms of gas yield, carbon conversion and H_2/CO ratio.

Gas yields and carbon conversions from devolatilization tests with ILM, SIB and LD, compared to that of sand, suggested that OCs made a difference in devolatilization only at the highest tested temperature, i.e., 900 °C. This temperature appeared as the most interesting in the range 700–900 °C, from the point of view of CLG and subsequent Fischer-Tropsch reaction (hypothesized in the CLARA project): it maximized the content of H_2 and CO, as well as their ratio (close or equal to 1), at the expense of gaseous hydrocarbons.

A simplified kinetic modelling approach was proposed, which purposely investigated the overall conversion phenomenon of devolatilization in a bubbling bed, lumping external heat transfer, intra-particle heat transfer and intrinsic devolatilization kinetics. The data obtained by this kinetic analysis reabsorbed part of the experimental uncertainty (highlighted by related standard deviations), so helped to evidence some trends: OCs had a positive contribution in the conversion of both WSP and RPR, as they involved higher specific reaction rates in comparison to the inert bubbling bed of sand. Kinetic data suggested that ILM ensured the fastest conversion, all other condition being equal.

This work might do the underground for future developments. Collected data could be used in mathematical models which describe CLG. In addition, the straightforward laboratory-scale experiments of this work may serve as a screening to choose promising

combinations of OCs and residual biomasses for more complex CLG tests, at higher scales and relevant industrial conditions; this would allow focusing the necessary characterization efforts (e.g., textural properties of fresh and spent solids) only on the most interesting cases. In conclusion, the methods used in this work are fully general and can be applied to study new kinds of biomass and OCs.

Author Contributions: Conceptualization, K.G. and A.D.G.; methodology, K.G. and A.D.G.; software, A.D.G. and S.L.; validation, K.G. and A.D.G.; formal analysis, K.G. and A.D.G.; investigation, K.G., A.D.G. and S.L.; resources, K.G.; data curation, A.D.G. and S.L.; writing—original draft preparation, A.D.G.; writing—review and editing, K.G. and A.D.G.; visualization, A.D.G. and S.L.; supervision, K.G.; project administration, K.G.; funding acquisition, K.G. All authors have read and agreed to the published version of the manuscript.

Funding: This research and the APC were funded by the Horizon 2020 Framework program of the European Union, CLARA project, G.A. 817841.

Institutional Review Board Statement: Not applicable.

Informed Consent Statement: Not applicable.

Data Availability Statement: The data presented in this study are available on request from the corresponding author.

Acknowledgments: The production and characterization of biomass pellets by the research team of National Renewable Energy Centre of Spain (CENER) is acknowledged, as well as the provision of oxygen carriers by Chalmers University of Technology (Göteborg, Sweden), both occurred within the CLARA project. The authors warmly thank Giampaolo Antonelli for his technical support.

Conflicts of Interest: The authors declare no conflict of interest. The funders had no role in the design of the study; in the collection, analyses, or interpretation of data; in the writing of the manuscript, or in the decision to publish the results.

Appendix A

For a given devolatilization tests, available experimental data consisted of: pellet mass (m_p), pellet composition [38], produced flow rates of H_2, CO, CO_2, CH_4 as functions of time ($F_{i,out}$).

Basing on the same principle of the one-component model (Figure 2), let us identify two groups as two lumped gaseous products: the C atoms transferred from the biomass pellet into gaseous products CO, CO_2, CH_4 ($n_{C,g}(t)$, Equation (A1)) and the H atoms with the same fate in H_2, CH_4 ($n_{H,g}(t)$, Equation (A2)):

$$n_{C,g}(t) = \int_0^t \left(F_{CO,out}(\tau) + F_{CO_2,out}(\tau) + F_{CH_4,out}(\tau)\right)d\tau = \int_0^t F_{C,g}(\tau)d\tau \quad \text{(A1)}$$

$$n_{H,g}(t) = \int_0^t \left(2F_{H_2,out}(\tau) + 4F_{CH_4,out}(\tau)\right)d\tau = \int_0^t F_{H,g}(\tau)d\tau \quad \text{(A2)}$$

Let us then identify the conversions, as functions of time, of C and H atoms from biomass into H_2, CO, CO_2, CH_4 ($\chi_C(t)$, Equation (A3) and $\chi_H(t)$, Equation (A4), respectively); these quantities were adopted as dependent variables in the SFOR model (Equation (5)) with the form proposed by Jand and Foscolo [30], obtaining the unsteady-state mole balances for C and H (Equations (A5) and (A6), respectively).

$$\chi_C(t) = \frac{\left(12\ \mathrm{g\ mol^{-1}}\right) \times n_{C,g}(t)}{m_p\left(1 - \frac{\%moisture_{ar}}{100}\right)\left(1 - \frac{\%ash_{db}}{100}\right)\left(\frac{\%C_{daf}}{100}\right)} \tag{A3}$$

$$\chi_H(t) = \frac{\left(1\ \mathrm{g\ mol^{-1}}\right) \times n_{H,g}(t)}{m_p\left(1 - \frac{\%moisture_{ar}}{100}\right)\left(1 - \frac{\%ash_{db}}{100}\right)\left(\frac{\%H_{daf}}{100}\right) + \frac{2\times\left(1\ \mathrm{g\ mol^{-1}}\right)}{\left(18\ \mathrm{g\ mol^{-1}}\right)}\left(m_p\frac{\%moisture_{ar}}{100}\right)} \tag{A4}$$

$$\frac{d\chi_C(t)}{dt} = k_C(T)\cdot(1 - \chi_C(t)) \quad with \quad k_C(T) = A_C \exp\left(-\frac{E_{a,C}}{R\,T}\right) \tag{A5}$$

$$\frac{d\chi_H(t)}{dt} = k_H(T)\cdot(1 - \chi_H(t)) \quad with \quad k_H(T) = A_H \exp\left(-\frac{E_{a,H}}{R\,T}\right) \tag{A6}$$

These balances, integrated by separation of variables, allowed the calculation of specific reaction rates k_C and k_H for each devolatilization experiment, by the linear regression in the plots $\ln(1 - \chi_C(t))$ vs. t and $\ln(1 - \chi_H(t))$ vs. t, considering a 10- or 8-points neighborhood centered on the maximum of $F_{H2,out}(t)$. This choice ensured the internal coherence when comparing kinetic data from different tests, as all cases were considered at the maximum of their gas release rate; in addition, data at this maximum descended from the most quantitatively substantial measurements in the first part of each devolatilization.

In turn, thanks to experiments at different temperatures (T), pre-exponential factors (A_C and A_H) and activation energies ($E_{a,C}$ and $E_{a,H}$) were calculated by linear regression in the plots $\ln k_C(T)$ vs. $1/RT$ and $\ln k_H(T)$ vs. $1/RT$, with T in Kelvin.

Appendix B

This appendix summarizes, in the form of tables, the numerical results discussed in this manuscript: Tables A1 and A2 show the experimental data of devolatilization tests, discussed in the main text and reported as histograms in Figures 4 and 5; Tables A3 and A4 show the experimental kinetic constants k_C and k_H obtained according to Section 2.4 and Appendix A.

Table A1. Experimental results of WSP devolatilization tests as functions of temperature and kind of bed material (av: average of results from the three individual pellets; stdev: standard deviation of results from the three individual pellets).

Bed	T	η^{av}		λ^{av}		$\chi^{av}{}_C$		$Y^{av}{}_{H2}$		$Y^{av}{}_{C3H8equiv}$		$Y^{av}{}_{CO}$		$Y^{av}{}_{CO2}$		$Y^{av}{}_{CH4}$	
	(°C)	(mol_{gas} $g_{biomass}{}^{-1}$)		(mol_{H2} $mol_{CO}{}^{-1}$)		(%)		(mol% dry N_2-free)		(mol% dry N_2-free)		(mol% dry N_2-free)		(mol% dry N_2-free)		(mol% dry N_2-free)	
		av	stdev	av	stdev	av	stdev	av	stdev	av	stdev	av	stdev	av	stdev	av	stdev
sand	700	0.017	0.002	0.32	0.03	58.8	2.1	12.6	1.3	16.0	3.1	39.1	0.4	15.9	0.7	16.3	1.3
	800	0.026	0.005	0.66	0.08	69.2	7.8	24.3	2.2	8.9	2.2	36.7	1.2	15.3	0.3	14.7	1.0
	900	0.035	0.001	0.96	0.02	72.9	1.3	36.3	1.8	3.7	0.4	37.7	1.3	10.7	1.5	11.5	1.3
ILM	700	0.016	0.006	0.30	0.06	53.6	16.2	11.7	3.1	15.4	5.3	39.1	2.7	16.3	0.1	17.5	0.7
	800	0.021	0.003	0.62	0.03	56.9	5.9	23.1	1.5	7.3	1.2	37.0	0.6	17.0	1.0	15.5	0.8
	900	0.038	0.003	0.84	0.05	81.7	9.7	32.8	1.8	3.2	0.8	38.9	0.0	12.3	0.5	12.8	1.4
SIB	700	0.017	0.001	0.26	0.07	55.5	2.9	10.1	2.2	9.9	0.2	39.0	1.8	25.6	0.7	15.3	0.3
	800	0.028	0.004	0.67	0.04	71.4	9.1	25.5	1.6	6.4	0.9	38.0	1.2	17.3	0.5	12.7	1.0
	900	0.040	0.003	0.90	0.07	82.2	4.1	36.1	2.6	3.6	1.1	40.1	1.1	10.1	0.80	10.1	1.0
LD	700	0.018	0.002	0.44	0.08	55.5	4.9	13.3	1.7	10.2	0.9	30.6	1.6	30.1	0.7	15.7	1.0
	800	0.025	0.002	0.65	0.06	67.8	3.7	21.6	1.6	7.4	0.2	33.1	1.6	24.9	2.9	13.0	1.1
	900	0.042	0.000	1.03	0.03	80.7	2.55	39.8	1.7	2.9	0.5	38.6	0.4	9.1	1.0	9.6	0.9

Table A2. Experimental results of RPR devolatilization tests as functions of temperature and kind of bed material (av: average of results from the three individual pellets; stdev: standard deviation of results from the three individual pellets).

Bed	T	η^{av}		λ^{av}		$\chi^{av}{}_{C}$		$Y^{av}{}_{H2}$		$Y^{av}{}_{C3H8equiv}$		$Y^{av}{}_{CO}$		$Y^{av}{}_{CO2}$		$Y^{av}{}_{CH4}$	
	(°C)	(mol_{gas} $g_{biomass}{}^{-1}$)		(mol_{H2} $mol_{CO}{}^{-1}$)		(%)		(mol% dry N_2-free)		(mol% dry N_2-free)		(mol% dry N_2-free)		(mol% dry N_2-free)		(mol% dry N_2-free)	
		av	stdev	av	stdev	av	stdev	av	stdev	av	stdev	av	stdev	av	stdev	av	stdev
sand	700	0.019	0.001	0.37	0.04	54.0	0.4	15.4	1.2	12.5	0.9	41.2	1.6	13.7	0.6	17.2	0.7
	800	0.030	0.002	0.71	0.05	66.2	5.1	26.9	1.6	7.3	0.9	38.1	0.3	12.2	0.6	15.6	2.6
	900	0.039	0.005	0.97	0.02	67.4	4.8	38.2	1.4	2.9	0.9	39.4	0.8	8.4	1.1	11.0	0.1
ILM	700	0.018	0.002	0.31	0.04	50.4	3.5	13.5	1.6	11.8	2.1	43.2	1.0	13.9	0.3	17.5	1.3
	800	0.025	0.003	0.59	0.09	57.2	6.2	23.0	1.8	6.9	1.3	39.1	3.0	13.3	0.5	17.7	1.2
	900	0.040	0.002	0.88	0.02	71.3	3.7	35.3	0.9	2.6	0.2	40.3	0.3	9.9	0.3	11.8	0.5
SIB	700	0.019	0.000	0.30	0.01	51.0	0.7	12.4	0.2	9.1	0.5	41.7	0.8	21.0	0.5	15.9	0.2
	800	0.023	0.001	0.67	0.07	53.0	0.8	25.4	1.2	7.5	0.9	37.1	2.3	15.3	0.9	14.6	0.7
	900	0.041	0.002	0.95	0.05	70.2	4.7	38.0	1.3	2.6	0.7	40.2	1.0	8.9	0.3	10.3	0.4
LD	700	0.018	0.002	0.42	0.07	48.3	3.7	13.1	1.1	10.9	2.0	31.2	2.4	30.5	4.6	14.2	1.2
	800	0.029	0.003	0.67	0.05	62.5	4.6	23.3	0.8	6.0	1.1	35.0	3.6	23.9	5.3	11.8	1.3
	900	0.036	0.008	1.04	0.07	63.1	12.8	38.8	1.784	4.3	1.1	37.2	2.2	9.5	1.0	10.2	1.3

Table A3. Kinetic constants k_C and k_H obtained according to Section 2.4 and Appendix A for WSP.

		Sand		ILM		SIB		LD	
T	Pellet	k_C	k_H	k_C	k_H	k_C	k_H	k_C	k_H
(°C)	[#]	(min^{-1})	(min^{-1})	(min^{-1})	(min^{-1})	(min^{-1})	(min^{-1})	(min^{-1})	(min^{-1})
700	1	0.338	0.205	0.454	0.288	0.472	0.230	0.389	0.232
	2	0.391	0.256	0.762	0.473	0.544	0.276	0.467	0.294
	3	0.372	0.248	0.501	0.322	0.558	0.313	0.400	0.255
800	1	0.548	0.458	0.561	0.428	0.614	0.496	0.564	0.437
	2	0.501	0.397	0.652	0.526	0.653	0.583	0.576	0.398
	3	0.599	0.522	0.637	0.521	0.558	0.476	0.507	0.388
900	1	0.539	0.577	1.137	1.050	0.683	0.791	0.752	1.040
	2	0.581	0.687	0.784	0.817	0.820	0.953	0.714	0.937
	3	0.505	0.557	0.957	0.998	0.927	1.100	0.687	0.894

Table A4. Kinetic constants k_C and k_H obtained according to Section 2.4 and Appendix A for RPR.

		Sand		ILM		SIB		LD	
T	Pellet	k_C	k_H	k_C	k_H	k_C	k_H	k_C	k_H
(°C)	[#]	(min^{-1})	(min^{-1})	(min^{-1})	(min^{-1})	(min^{-1})	(min^{-1})	(min^{-1})	(min^{-1})
700	1	0.337	0.243	0.472	0.324	0.493	0.299	0.357	0.243
	2	0.338	0.260	0.467	0.333	0.498	0.301	0.397	0.268
	3	0.340	0.259	0.499	0.348	0.451	0.276	0.351	0.233
800	1	0.500	0.478	0.496	0.414	0.450	0.449	0.478	0.425
	2	0.484	0.476	0.505	0.542	0.434	0.396	0.538	0.430
	3	0.450	0.427	0.580	0.511	0.440	0.420	0.438	0.372
900	1	0.480	0.598	0.741	0.851	0.711	0.986	0.395	0.542
	2	0.550	0.749	0.812	0.951	0.709	0.919	0.682	0.875
	3	0.450	0.549	0.755	0.908	0.625	0.839	0.851	1.182

References

1. Molino, A.; Larocca, V.; Chianese, S.; Musmarra, D. Biofuels Production by Biomass Gasification: A Review. *Energies* **2018**, *11*, 811. [CrossRef]
2. Weber, G.; Di Giuliano, A.; Rauch, R.; Hofbauer, H. Developing a simulation model for a mixed alcohol synthesis reactor and validation of experimental data in $IPSE_{pro}$. *Fuel Process. Technol.* **2016**, *141*, 167–176. [CrossRef]
3. Groppi, G.; Tronconi, E.; Forzatti, P.; Berg, M. Mathematical modelling of catalytic combustors fuelled by gasified biomasses. *Catal. Today* **2000**, *59*, 151–162. [CrossRef]
4. Zhang, Y.; Xiao, J.; Shen, L. Simulation of methanol production from biomass gasification in interconnected fluidized beds. *Ind. Eng. Chem. Res.* **2009**, *48*, 5351–5359. [CrossRef]
5. European Union Directives. Directive 2009/28/EC of the European Parliament and of the Council of 23 April 2009 on the promotion of the use of energy from renewable sources and amending and subsequently repealing Directives 2001/77/EC and 2003/30/EC. *Off. J. Eur. Union* **2009**, *L140/16*, 1–47.
6. Congress of United States. *Energy Independence and Security Act of 2007*; Congress of United States: Washington, DC, USA, 2007; pp. 110–140.
7. Obama, B. The irreversible momentum of clean energy. *Science* **2017**, *355*, 126–129. [CrossRef]
8. Marris, E. Why young climate activists have captured the world's attention. *Nature* **2019**, *573*, 471–472. [CrossRef]
9. United Nations Paris Agreement, 21st Conf. Parties. Available online: https://treaties.un.org/doc/Treaties/2016/02/20160215%2006-03%20PM/Ch_XXVII-7-d.pdf (accessed on 30 October 2019).
10. COP24 COP 24 Katowice 2018. Available online: https://cop24.gov.pl/ (accessed on 19 April 2019).
11. CLARA Chemical Looping Gasification for Sustainable Production of Biofuels. Available online: https://clara-h2020.eu/ (accessed on 7 July 2020).
12. Di Giuliano, A.; Funcia, I.; Pérez-Vega, R.; Gil, J.; Gallucci, K. Novel application of pretreatment and diagnostic method using dynamic pressure fluctuations to resolve and detect issues related to biogenic residue ash in chemical looping gasification. *Processes* **2020**, *8*, 1137. [CrossRef]
13. Ge, H.; Guo, W.; Shen, L.; Song, T.; Xiao, J. Biomass gasification using chemical looping in a 25kWth reactor with natural hematite as oxygen carrier. *Chem. Eng. J.* **2016**, *286*, 174–183. [CrossRef]
14. Higman, C.; van der Burgt, M. *Gasification*, 2nd ed.; Elsevier: Burlington, VT, USA, 2008; ISBN 9780750685283.
15. Ohlemüller, P.; Ströhle, J.; Epple, B. Chemical looping combustion of hard coal and torrefied biomass in a 1 MWth pilot plant. *Int. J. Greenh. Gas Control* **2017**, *65*, 149–159. [CrossRef]
16. Adanez, J.; Abad, A.; Garcia-Labiano, F.; Gayan, P.; De Diego, L.F. Progress in chemical-looping combustion and reforming technologies. *Prog. Energy Combust. Sci.* **2012**, *38*, 215–282. [CrossRef]
17. Berguerand, N.; Lyngfelt, A. Design and operation of a 10 kWth chemical-looping combustor for solid fuels Testing with South African coal. *Fuel* **2008**, *87*, 2713–2726. [CrossRef]
18. Leion, H.; Mattisson, T.; Lyngfelt, A. Solid fuels in chemical-looping combustion. *Int. J. Greenh. Gas Control* **2008**, *2*, 180–193. [CrossRef]
19. Ströhle, J.; Orth, M.; Epple, B. Chemical looping combustion of hard coal in a 1 MWthpilot plant using ilmenite as oxygen carrier. *Appl. Energy* **2015**, *157*, 288–294. [CrossRef]
20. Ge, H.; Guo, W.; Shen, L.; Song, T.; Xiao, J. Experimental investigation on biomass gasification using chemical looping in a batch reactor and a continuous dual reactor. *Chem. Eng. J.* **2016**, *286*, 689–700. [CrossRef]
21. Wei, G.; He, F.; Huang, Z.; Zheng, A.; Zhao, K.; Li, H. Continuous operation of a 10 kWth chemical looping integrated fluidized bed reactor for gasifying biomass using an iron-based oxygen carrier. *Energy Fuels* **2015**, *29*, 233–241. [CrossRef]
22. Huang, Z.; He, F.; Zhao, K.; Feng, Y.; Zheng, A.; Chang, S.; Zhao, Z.; Li, H. Natural iron ore as an oxygen carrier for biomass chemical looping gasification in a fluidized bed reactor. *J. Anal. Calorim.* **2014**, *116*, 1315–1324. [CrossRef]
23. Huang, Z.; He, F.; Zhu, H.; Chen, D.; Zhao, K.; Wei, G.; Feng, Y.; Zheng, A.; Zhao, Z.; Li, H. Thermodynamic analysis and thermogravimetric investigation on chemical looping gasification of biomass char under different atmospheres with Fe2O3 oxygen carrier. *Appl. Energy* **2015**, *157*, 546–553. [CrossRef]
24. Guo, Q.; Cheng, Y.; Liu, Y.; Jia, W.; Ryu, H.J. Coal chemical looping gasification for syngas generation using an iron-based oxygen carrier. *Ind. Eng. Chem. Res.* **2014**, *53*, 78–86. [CrossRef]
25. Pour, N. Status of bioenergy with carbon capture and storage-potential and challenges. In *Bioenergy with Carbon Capture and Storage: Using Natural Resources for Sustainable Development*; Magalhaes Pires, J.C., da Cunha Goncalves, A.L., Eds.; Elsevier: London, UK, 2019; pp. 85–107. ISBN 9780128162293.
26. Cazzaniga, N.E.; Jonsson, R.; Palermo, D.; Camia, A. *Sankey Diagrams of Woody Biomass Flows in the EU-28*; EC Joint Research Centre, Publications Office of the European Union: Luxembourg, 2019; JRC115777. [CrossRef]
27. S2Biom Project Deliverable 8.2. Available online: https://www.s2biom.eu/images/Publications/D8.2_S2Biom_Vision_for_1_billion_tonnes_biomass_2030.pdf (accessed on 1 July 2019).
28. International Renewable Energy Agency. *Solid Biomass Supply for Heat and Power: Technology Brief, International Renewable Energy Agency*; International Renewable Energy Agency: Abu Dahbi, UAE, 2019; ISBN 9789292601072.
29. Transport & Environment; BirdLife International. How Much Sustainable Biomass Does Europe Have in 2030? Available online: https://www.transportenvironment.org/sites/te/files/publications/How%20much%20sustainable%20biomass%20available%20in2030_FINAL.pdf (accessed on 18 July 2020).

30. Jand, N.; Foscolo, P.U. Decomposition of wood particles in fluidized beds. *Ind. Eng. Chem. Res.* **2005**, *44*, 5079–5089. [CrossRef]
31. Milne, T.; Agblevor, F.; Davis, M.; Deutch, S.; Johnson, D. A Review of the Chemical Composition of Fast-Pyrolysis Oils from Biomass. In *Developments in Thermochemical Biomass Conversion*; Springer: Dordrecht, The Netherlands, 1997; pp. 409–424.
32. Belgiorno, V.; De Feo, G.; Della Rocca, C.; Napoli, R.M.A. Energy from gasification of solid wastes. *Waste Manag.* **2003**, *23*, 1–15. [CrossRef]
33. Bryden, K.M.; Hagge, M.J. Modeling the combined impact of moisture and char shrinkage on the pyrolysis of a biomass particle. *Fuel* **2003**, *82*, 1633–1644. [CrossRef]
34. Grønli, M.G.; Várhegyi, G.; Di Blasi, C. Thermogravimetric analysis and devolatilization kinetics of wood. *Ind. Eng. Chem. Res.* **2002**, *41*, 4201–4208. [CrossRef]
35. Rath, J.; Steiner, G.; Wolfinger, M.G.; Staudinger, G. Tar cracking from fast pyrolysis of large beech wood particles. *J. Anal. Appl. Pyrolysis* **2002**, *62*, 83–92. [CrossRef]
36. Conesa, J.A.; Marcilla, A.; Caballero, J.A.; Font, R. Comments on the validity and utility of the different methods for kinetic analysis of thermogravimetric data. *J. Anal. Appl. Pyrolysis* **2001**, *58–59*, 617–633. [CrossRef]
37. Unidad de Pretratamiento Cener BIO2C. Available online: https://www.bio2c.es/es/unidad-de-pretratamiento/ (accessed on 19 July 2020).
38. Schipfer, F.; Haas, R.; Funcia, I.; Gil, J.; Bojner, U.; Ströhle, J.; Buschsieweke, F.; Wallus, S.; Aichernig, C. Deliverable D1.1 Analysis of Selected Feedstock. Available online: https://clara-h2020.eu/category/deliverable/ (accessed on 16 December 2020).
39. Larsson, A.; Israelsson, M.; Lind, F.; Seemann, M.; Thunman, H. Using ilmenite to reduce the tar yield in a dual fluidized bed gasification system. *Energy Fuels* **2014**, *28*, 2632–2644. [CrossRef]
40. Mattison, T.; Hildor, F.; Li, Y.; Linderholm, C. Negative emissions of carbon dioxide through chemical-looping combustion (CLC) and gasification (CLG) using oxygen carriers based on manganese and iron. *Mitig. Adapt. Strat. Glob. Chang.* **2020**, *25*, 497–517. [CrossRef]
41. Gibilaro, L.G. *Fluidization Dynamics*, 1st ed.; Butterworth-Heinemann: Oxford, UK, 2010.
42. Grace, R.J. Fluidized Bed Hydrodynamics. In *Handbook of Multiphase Systems*; Hetsroni, G., Ed.; Hemisphere: Washington, DC, USA, 1982; pp. 8-5–8-64.
43. Yang, W. *Handbook of Fluidization and Fluid-Particle Systems*; Marcel Dekker Inc.: New York, NY, USA, 2003.
44. Di Blasi, C. Modeling chemical and physical processes of wood and biomass pyrolysis. *Prog. Energy Combust. Sci.* **2008**, *34*, 47–90. [CrossRef]
45. Shafizadeh, F.; Chin, P.P.S. Thermal Deterioration of Wood. In *Wood Technology: Chemical Aspects*; ACS Symposium Series; American Chemical Society: Washington, DC, USA, 1977; pp. 57–81.
46. Simone, M.; Biagini, E.; Galletti, C.; Tognotti, L. Evaluation of global biomass devolatilization kinetics in a drop tube reactor with CFD aided experiments. *Fuel* **2009**, *88*, 1818–1827. [CrossRef]
47. Thurner, F.; Mann, U. Kinetic Investigation of Wood Pyrolysis. *Ind. Eng. Chem. Process Des. Dev.* **1981**, *20*, 482–488. [CrossRef]
48. Scala, F. Particle agglomeration during fluidized bed combustion: Mechanisms, early detection and possible countermeasures. *Fuel Process. Technol.* **2018**, *171*, 31–38. [CrossRef]
49. Hildor, F.; Leion, H.; Linderholm, C.J.; Mattisson, T. Steel converter slag as an oxygen carrier for chemical-looping gasification. *Fuel Process. Technol.* **2020**, *210*, 106576. [CrossRef]
50. Kersten, S.R.A.; Wang, X.; Prins, W.; Van Swaaij, W.P.M. Biomass pyrolysis in a fluidized bed reactor. Part 1: Literature review and model simulations. *Ind. Eng. Chem. Res.* **2005**, *44*, 8773–8785. [CrossRef]
51. Wang, X.; Kersten, S.R.A.; Prins, W.; Van Swaaij, W.P.M. Biomass pyrolysis in a fluidized bed reactor. Part 2: Experimental validation of model results. *Ind. Eng. Chem. Res.* **2005**, *44*, 8786–8795. [CrossRef]